European Journal of Pharmaceutics and Biopharmaceutics 137 (2019) 86–94

Contents lists available at ScienceDirect

European Journal of Pharmaceutics and Biopharmaceutics

journal homepage: www.elsevier.com/locate/ejpb

Research paper

Hyaluronic acid functionalized nanoparticles loaded with IR780 and DOX for cancer chemo-phototherapy

Cátia G. Alves[a], Duarte de Melo-Diogo[a,*], Rita Lima-Sousa[a], Elisabete C. Costa[a], Ilídio J. Correia[a,b,*]

[a] CICS-UBI – Centro de Investigação em Ciências da Saúde, Universidade da Beira Interior, 6200-506 Covilhã, Portugal
[b] CIEPQPF – Departamento de Engenharia Química, Universidade de Coimbra, Rua Sílvio Lima, 3030-790 Coimbra, Portugal

ARTICLE INFO

Keywords:
Cancer
Chemotherapy
Doxorubicin
IR780
Photothermal therapy
Polymeric nanoparticles

ABSTRACT

IR780 is a near infrared (NIR) dye with a huge potential to be applied in cancer phototherapy and imaging. However, IR780 poor water solubility and acute cytotoxicity limit its direct use in cancer theragnostic. Herein, a novel Hyaluronic acid (HA)-based amphiphilic polymer was used, for the first time, in the preparation of polymeric nanoparticles (HPN) encapsulating IR780 aimed to be applied in breast cancer therapy. Furthermore, HPN co-encapsulating IR780 and Doxorubicin (DOX) were also produced in order to further enhance the therapeutic effectiveness of this nanoformulation. The results revealed that HPN were able to successfully encapsulate IR780 (IR-HPN) and the IR780-DOX combination (IR/DOX-HPN). Furthermore, the encapsulation of IR780 in HPN improved its absorption at 808 nm by about 2.2-fold, thereby enhancing its photothermal potential, as well as its cytocompatibility. The 2D *in vitro* cell uptake studies demonstrated that the nanostructures displayed a higher internalization by breast cancer cells than by normal cells. In addition, the assays performed in 3D *in vitro* models of breast cancer revealed that HPN can penetrate into spheroids. Furthermore, the 3D *in vitro* studies also demonstrated that the combined application of IR-HPN and NIR light was unable to induce cytotoxicity on spheroids. In contrast, IR/DOX-HPN produced a decrease on spheroids cells' viability, and their combination with NIR light induced an even stronger therapeutic effect, thus revealing the potential of these nanoparticles for cancer chemo-phototherapy.

1. Introduction

Breast cancer is one of the deadliest diseases among women [16]. The currently available treatments for this type of cancer comprise radiotherapy and chemotherapy. However, these therapies are severely limited by their poor efficacy and non-specificity towards cancer cells, which can lead to severe side effects [6].

To improve the effectiveness of cancer treatments, researchers have been investigating different approaches. In particular, phototherapies using IR780 have been demonstrating promising results in *in vitro* and *in vivo* assays [1]. This small molecule has an absorption peak at 780 nm, producing upon interaction with near infrared light (750–1000 nm, NIR) a temperature increase (photothermal therapy) and/or reactive oxygen species (photodynamic therapy), which can induce damage on cancer cells [39]. Furthermore, IR780 also emits fluorescence in the NIR window [53]. Due to this fact, this agent has a great potential for NIR imaging applications since its signals can be visualized with minimal detection of tissues' auto-fluorescence [1]. In fact, the optical properties of IR780 are superior to those of Indocyanine Green (an FDA approved molecule) [53] and of other NIR dyes under

Abbreviations: ANOVA, Analysis of Variance; CLSM, Confocal Laser Scanning Microscopy; DLS, Dynamic Light Scattering; DMEM-F12, Dulbecco's Modified Eagle's Medium-F12; DMSO, Dimethyl Sulfoxide; DOX, Doxorubicin; EDC, 1-Ethyl-3-(3-dimethylaminopropyl)carbodiimide; EE, Encapsulation Efficiency; EPR, Enhanced Permeability and Retention; FBS, Fetal Bovine Serum; HA, Hyaluronic Acid; HA-*g*-PMAO, HA grafted PMAO; HPN, HA-based Polymeric Nanoparticles; IC_{50}, Half Maximal Inhibitory Concentration; IR/DOX-HPN, IR780-DOX loaded HPN; IR-HPN, IR780 loaded HPN; LC, Loading Content; MCF-7, Michigan Cancer Foundation-7; NHDF, Normal Human Dermal Fibroblasts; NHS, *N*-Hydroxysuccinimide; NIR, Near Infrared; ns, Non-significant; PBS, Phosphate Buffered Saline; PDI, Polydispersity Index; PEG, Poly(ethylene glycol); PI, Propidium Iodide; PMAO, Poly(maleic anhydride-*alt*-1-octadecene); S.D., Standard Deviation; TEM, Transmission Electron Microscopy

* Corresponding authors at: CICS-UBI – Centro de Investigação em Ciências da Saúde, Universidade da Beira Interior, 6200-506 Covilhã, Portugal (I.J. Correia and D. de Melo-Diogo).
E-mail addresses: demelodiogo@fcsaude.ubi.pt (D. de Melo-Diogo), icorreia@ubi.pt (I.J. Correia).

https://doi.org/10.1016/j.ejpb.2019.02.016
Received 10 September 2018; Received in revised form 21 January 2019; Accepted 19 February 2019
Available online 20 February 2019
0939-6411/

investigation (*e.g.* IR783, IRDye® 800CW) [1], thereby attesting its potential for application in cancer theragnostic.

Despite the potential of IR780, this NIR molecule presents critical limitations such as low solubility and acute cytotoxicity, which hinder its direct use for cancer theragnostic [39]. These drawbacks can be surpassed by encapsulating IR780 within nanocarriers, namely in the hydrophobic core of polymeric nanoparticles [3,20,44]. Furthermore, nanoparticles can also accommodate drugs in their core (*e.g.* Doxorubicin (DOX)) [32], thus being a versatile platform for cancer chemo-phototherapy. However, the majority of the amphiphilic polymers used to formulate polymeric nanoparticles (*e.g.* poly(ethylene glycol) (PEG)-based amphiphilic materials) do not have targeting motifs that can improve nanoparticles' selectivity towards cancer cells. In this way, polymeric nanoparticles generally do not have intrinsically the capacity to induce a cancer cell-selective therapeutic effect.

In this work, a novel Hyaluronic acid (HA)-based amphiphilic polymer was explored, to the best of our knowledge for the first time, in the preparation of polymeric nanoparticles encapsulating IR780 and DOX aimed to be used for breast cancer chemo-phototherapy. HA was selected as the hydrophilic segment of the amphiphilic polymer due to its ability to bind to CD44 receptors, which are overexpressed on cancer cells' membrane [8,45]. Additionally, this receptor is in a quiescent state in normal cells, *i.e.*, it does not have the ability to bind to HA [50]. Deacetylated HA was then grafted onto hydrolysed poly(maleic anhydride-*alt*-1-octadecene) (PMAO) in order to produce the amphiphilic polymer (HA grafted PMAO (HA-*g*-PMAO)) required for nanoparticles formulation. The results revealed that the HA-based polymeric nanoparticles (HPN) encapsulated successfully the IR780 (IR-HPN) and the IR780-DOX combination (IR/DOX-HPN). The encapsulation of IR780 in HPN improved its absorption at 808 nm by about 2.2-fold, thereby enhancing its photothermal potential, as well as its cytocompatibility. The 2D *in vitro* cell uptake studies showed that the nanostructures displayed a higher internalization by breast cancer cells than by normal cells. In addition, the assays performed in 3D *in vitro* models of breast cancer revealed that HPN can penetrate into spheroids. Furthermore, the 3D *in vitro* studies also demonstrated that the combined application of IR-HPN and NIR light was unable to induce cytotoxicity on spheroids. In contrast, IR/DOX-HPN produced a decrease on spheroids cells' viability to 54%. Moreover, the combined action of IR/DOX-HPN and NIR light induced an even stronger therapeutic effect by reducing spheroids cells' viability to 34%, thereby demonstrating the potential of HPN for cancer chemo-phototherapy.

2. Materials and methods

2.1. Materials

Michigan Cancer Foundation-7 (MCF-7) cell line and Normal Human Dermal Fibroblast (NHDF) were obtained from ATCC (Middlesex, UK) and Promocell (Heidelber, Germany), respectively. Fetal Bovine Serum (FBS) was acquired from Biochrom AG (Berlin, Germany). 1-Ethyl-3-(3-dimethylaminopropyl) carbodiimide (EDC) was purchased from Merck (Darmstadt, Germany). DOX and HA Sodium Salt (8000–15000 Da) were obtained from Carbosynth (Berkshire, United Kingdom). Acetone, Dimethyl Sulfoxide (DMSO), methanol, Triton X-100 and Tween 80™ were acquired from Fisher Scientific (Oeiras, Portugal). Agarose was bought from Grisp (Porto, Portugal). Cell imaging plates were obtained from Ibidi GmbH (Munich, Germany). Cell culture plates and T-flasks were purchased from Thermo Fisher Scientific (Porto, Portugal). Dulbecco's Modified Eagle's Medium F12 (DMEM-F12), IR780 iodide, *N*-Hydroxysuccinimide (NHS), paraformaldehyde, PMAO (average Mn 30000–50000 Da), resazurin and trypsin were bought from Sigma-Aldrich (Sintra, Portugal). Calcein-AM, Hoechst 33342® and Propidium Iodide (PI) were obtained from Thermo Fisher Scientific (Porto, Portugal). Water used in all experiments was double deionized (0.22 μm filtered, 18.2 MΩ cm).

2.2. Methods

2.2.1. Formulation of IR-HPN and IR/DOX-HPN

HPN loaded with IR780 and DOX (IR/DOX-HPN) were prepared through the nanoprecipitation method as previously described by our group [39]. In brief, 1 mL of a Water:Acetone solution (1:1 (v/v)) containing HA-*g*-PMAO (5 mg mL^{-1}; the synthesis of HA-*g*-PMAO is described in the Supplementary Information), IR780 (125 μg) and DOX (125 μg) was added dropwise into water under stirring. After 2 h, the aqueous solution was recovered and dialyzed against water (500–1000 Da cut-off membrane; 2 h), yielding IR/DOX-HPN. The same protocol was used to prepare IR-HPN (using 250 μg of IR780).

2.2.2. Physicochemical characterization of IR-HPN and IR/DOX-HPN

HPN size distribution and zeta potential were evaluated by Dynamic Light Scattering (DLS) in a Zetasizer Nano ZS (Malvern Instruments Ltd., Worcestershire, UK). Transmission Electron Microscopy (TEM) was used to analyse the morphology of both HPN formulations. For such, the nanoformulations were stained with phosphotungstic acid (2% (w/v)) and were imaged in a Hitachi-HT7700 transmission electron microscope (Hitachi Ltd., Tokyo, Japan), at an accelerating voltage of 100 kV.

2.2.3. Encapsulation efficiency and loading content of IR780 and DOX

HPN ability to encapsulate IR780 and/or DOX was determined by UV–Vis absorption and fluorescence spectroscopies. First, HPN were freeze dried in a ScanVac CoolSafe (LaboGene ApS, Lynge, Denmark), and then were resuspended in methanol. Then, a standard curve of IR780 (in methanol) and samples' absorbance at 780 nm were used to determine the content of IR780 within the sample using an Evolution 201 UV–Visible spectrophotometer (Thermo Fisher Scientific Inc., Massachusetts, USA). In turn, the fluorescence emitted by the samples at 590 nm (λ_{ex} = 488 nm) and a standard curve of DOX (in methanol, λ_{ex} = 488 nm, λ_{em} = 590 nm) were employed to determine the content of DOX by using a Spectramax Gemini EM spectrofluorometer (Molecular Devices LLC, California, USA). HPN Encapsulation Efficiency (EE) and Loading Content (LC) were determined according to Eqs. (1) and (2):

$$EE(\%) = \frac{Weight\ of\ IR780\ or\ DOX\ encapsulated\ in\ HPN}{Weight\ of\ IR780\ or\ DOX\ initially\ fed} \times 100 \quad (1)$$

$$LC(\%) = \frac{Weight\ of\ IR780\ or\ DOX\ encapsulated\ in\ HPN}{Weight\ of\ loaded\ HPN} \times 100 \quad (2)$$

2.2.4. NIR Absorption, photothermal capability and release behaviour of HPN

The ability of IR-HPN and IR/DOX-HPN to interact with NIR light was evaluated by measuring the samples' absorbance in the 750–1000 nm wavelength range. For such, the absorption of IR-HPN and IR/DOX-HPN in water and in methanol after freeze-drying was determined (2.5 μg mL^{-1} of IR780 equivalents). The photothermal capability of HPN was characterized by evaluating the temperature variations induced by these nanoformulations (at different concentrations of IR780) during 5 min of NIR laser irradiation (808 nm, 1.7 W cm^{-2}). Temperature measurements were performed using a thermocouple thermometer. Water was used as control.

The IR780 and/or DOX cumulative release from HPN were characterized through a dialysis method as described elsewhere [33]. In brief, IR-HPN or IR/DOX-HPN formulations dispersed in 1 mL of release medium (Phosphate Buffered Saline (PBS) solution containing Tween 80 (0.1% (v/v)) at a pH of 7.4) were transferred into a dialysis tube (500–1000 Da molecular weight cut-off). Afterwards, the tube was immersed in 15 mL of release medium at 37 °C under stirring, and

samples were withdrawn at predetermined intervals to quantify the released IR780 and DOX. To assess the influence of the NIR light on compounds' release, HPN samples were also irradiated with NIR light for 5 min (808 nm, 1.7 W cm^{-2}) after the immersion of the dialysis tube in the release medium.

2.2.5. Cytocompatibility of IR-HPN

The cytocompatibility of IR-HPN towards MCF-7 (breast cancer cell model) and NHDF (normal cell model) was determined using the resazurin method, as previously described by our group [14]. For the assay, cells were seeded (1×10^4 cells/well) in 96 well-plates and were cultured in DMEM-F12 medium supplemented with 10% (v/v) FBS and 1% (v/v) streptomycin/gentamycin in a humidified incubator (37 °C, 5% CO_2). After 24 h, the culture medium was removed, and cells were incubated with fresh medium containing different concentrations of IR-HPN. After 24 and 48 h of incubation, the medium was replaced with fresh culture medium containing resazurin (10% (v/v)) and cells were incubated for 4 h in the dark (37 °C, 5% CO_2). Then, the fluorescence of resorufin (λ_{ex} = 560 nm; λ_{em} = 590 nm) was measured (Spectramax Gemini EM spectrofluorometer) in order to determine cells' viability. Cells solely incubated with medium and cells incubated with ethanol (70% (v/v)) were used as negative (K-) and positive (K+) controls, respectively.

2.2.6. Cellular uptake of IR-HPN and IR/DOX-HPN

The uptake of HPN was investigated in MCF-7 cells (CD44 receptor overexpressing cells [7,40,42]) and NHDF (which do not overexpress the CD44 receptor [36,50]) through Confocal Laser Scanning Microscopy (CLSM) and by taking advantage from the intrinsic fluorescence of IR780 and DOX. In brief, cells were seeded in μ-slide 8-well imaging plates (Ibidi GmbH, Munich, Germany) at a density of 1.5×10^4 cells/well. After 48 h, cells were incubated with culture medium containing IR-HPN (IR780: 2 μg mL^{-1}), IR/DOX-HPN (IR780/DOX: 2/1.10 μg mL^{-1}), free IR780 (2 μg mL^{-1}) and free DOX (1.10 μg mL^{-1}) during 4 h. Afterwards, the medium was discarded and cells were washed several times with a PBS solution. Then, cells were fixed with paraformaldehyde 4% for 15 min at room temperature and were washed twice with the PBS solution. Cells' nucleus were labelled with Hoechst 33342® for 45 min at 4 °C. Fluorescence images were acquired using a $\lambda_{ex}/\lambda_{em}$ of 405/410–499 (Hoechst 33342®), 488/534–622 (DOX) and 633/656–758 nm (IR780) in a Zeiss LSM 710 confocal microscope (Carl Zeiss AG, Oberkochen, Germany).

2.2.7. Phototherapeutic effect mediated by HPN in 2D cancer models

The phototherapeutic capability of HPN was determined using the resazurin method as described above [13]. In brief, MCF-7 cells were seeded (1×10^4 cells/well) in 96-well plates. After 24 h, the medium was replaced by fresh medium containing IR-HPN (IR780: 2 or 3.5 μg mL^{-1}) or IR/DOX-HPN (IR780/DOX: 2/1.10 μg mL^{-1} or 3.5/1.93 μg mL^{-1}). After 4 h of incubation, cells were irradiated with NIR light (808 nm, 1.7 W cm^{-2}) for 5 min. After totalling a 24 h incubation period, cells' viability was evaluated. Cells solely incubated with medium and cells incubated with ethanol (70% (v/v)) were used as negative (K-) and positive (K+) controls, respectively.

To visualize the phototherapeutic effect mediated by HPN, cells seeded as described in Section 2.2.6. were incubated with culture medium containing HPN (3.5 μg mL^{-1} of IR780 equivalents) during 4 h. Afterwards, cells were irradiated with NIR light (808 nm, 1.7 W cm^{-2}) for 5 min. Then, the medium was discarded, and cells were stained with Calcein-AM (enables the visualization of live cells) and PI (enables the visualization of dead cells) for 15 min according to the manufacturer's protocol. Fluorescence images were acquired using a $\lambda_{ex}/\lambda_{em}$ of 488/493–556 (Calcein-AM) and 561/566–719 nm (PI) in a Zeiss LSM 710 confocal microscope. Cells solely incubated with culture medium and cells incubated with Triton X-100 were used as controls for live and dead cells, respectively.

2.2.8. Penetration and phototherapeutic effect mediated by HPN in 3D cancer models

3D MCF-7 spheroids were produced as previously described by our group [10,19]. In brief, hydrogel structures with round-bottom microwells were produced by casting agarose gel (2% (w/v)) in a negative template (3D Petri Dish®, Microtissues Inc., Providence RI, US). MCF-7 cells were then seeded at a density of 1×10^6 cells/agarose structure, resulting in the formation of 81 spheroids/structure. 3D MCF-7 spheroids were grown for 10 days, reaching a mean diameter of 607 ± 63 μm (determined by using ImageJ software (National Institutes of Health)). During this period, spheroids were maintained in DMEM-F12 medium supplemented with 10% (v/v) FBS and 1% (v/v) streptomycin/gentamycin (37 °C, 5% CO_2) and the culture medium was exchanged every 2 days.

To characterize the penetration capacity of the nanoparticles in the spheroids, culture medium containing HPN (3 μg mL^{-1} of IR780 equivalents) was added to plates containing spheroids for 24 h [18]. Subsequently, spheroids were fixed with paraformaldehyde 4% and then were visualized by CLSM using the parameters described in Section 2.2.6. Z-stacks were collected with 5 μm intervals. The plots of the fluorescence intensity across the spheroids' diameter, at different penetration depths, were determined by using the ImageJ software as described in a previous publication of our group [12].

The phototherapeutic capability of HPN towards 3D spheroids was also determined using the resazurin method. In brief, the assembled spheroids were incubated with culture medium containing IR-HPN (IR780: 5 μg mL^{-1}) and IR/DOX-HPN (IR780/DOX: 5/2.76 μg mL^{-1}) for 24 h. Each experimental condition was assessed with 30 spheroids. Then, spheroids were irradiated with NIR light (808 nm, 1.7 W cm^{-2}) for 5 min. After 48 h, the medium was exchanged with fresh cell culture medium containing resazurin (10% (v/v)) and spheroids cells' viability was determined as described in Section 2.2.5.

2.2.9. Statistical analysis

To compare different groups, one-way analysis of variance (ANOVA) was used with the Student-Newman-Keuls test. A value of p lower than 0.05 ($p < 0.05$) was considered statistically significant. All data are presented as the mean ± standard deviation (S.D.).

3. Results and discussion

3.1. Formulation and characterization of IR-HPN and IR/DOX-HPN

The hydrophobicity and non-specific toxicity of IR780 and DOX may limit the direct application of these molecules in cancer chemo-phototherapy [1,41]. In this way, the amphiphilic polymer HA-*g*-PMAO was synthesized in order to be explored in the formulation of novel nanoparticles that can be used for the co-encapsulation of IR780 and DOX (characterization of HA-*g*-PMAO is reported in the Supplementary Information - Fig. S1–3). Furthermore, HA-*g*-PMAO nanoparticles may enable a selective cancer cell therapy mediated by the binding of the HA to the CD44 receptors, which are overexpressed on cancer cells' membrane (Fig. 1A).

HA-*g*-PMAO nanoparticles encapsulating IR780 (IR-HPN) were prepared through a nanoprecipitation method, revealing an average size of 173.5 ± 8.5 nm (n = 3; batch triplicates; Fig. 1B). The inclusion of the IR780-DOX combination in HA-*g*-PMAO nanoparticles (IR/DOX-HPN) increased slightly the nanoparticles' size to 198.9 ± 2.8 nm (n = 3; batch triplicates; Fig. 1B). The differences in the sizes of both formulations may be explained by the different hydrophobic interactions established in the nanoparticles' core. Nevertheless, the size of IR-HPN and IR/DOX-HPN is within the 100–200 nm range, suggesting their ability to passively accumulate in the tumor zone through the enhanced permeability and retention (EPR) effect [2]. Furthermore, the DLS analysis also revealed that IR-HPN and IR/DOX-HPN present very low polydispersity index (PDI) values of 0.139 ± 0.026 and

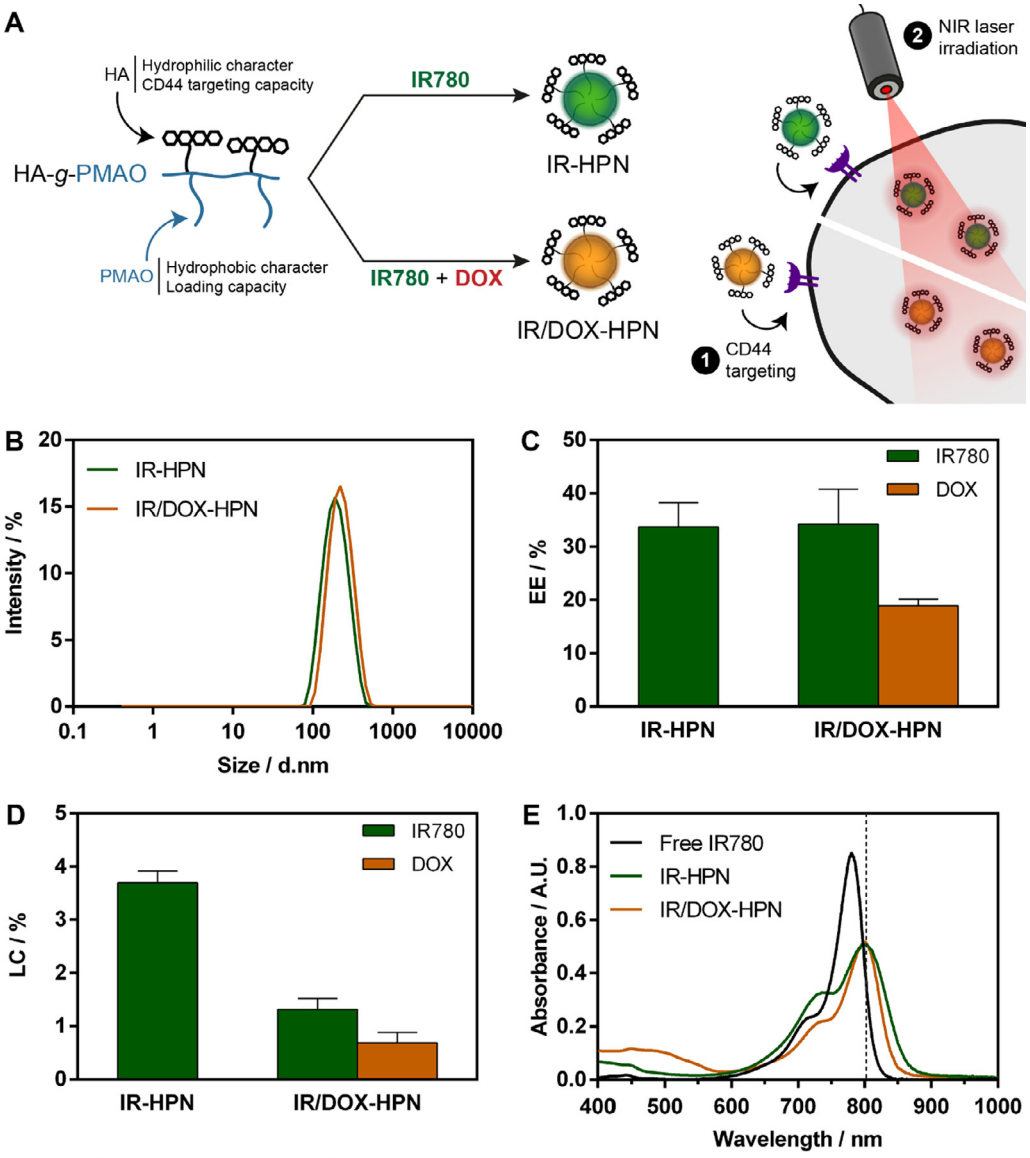

Fig. 1. Characterization of HPN physicochemical, loading and optical properties. Schematic representation of HPN assembly and application in cancer therapy (A). DLS size distribution of IR-HPN and IR/DOX-HPN (B). EE (C) and LC (D) of IR780 and/or DOX in IR-HPN and IR/DOX-HPN. Each bar represents mean ± S.D. (n = 3; batch triplicates). Absorption spectra of free IR780 (2.5 μg mL^{-1}; in methanol), IR-HPN and IR/DOX-HPN (2.5 μg mL^{-1} of IR780 equivalents; in water) (E).

0.119 ± 0.028, respectively. Such finding indicates that the nanoparticles have a monodisperse size distribution, further corroborating the efficiency of the nanoprecipitation method in the assembly of nanoparticles with suitable physicochemical properties for application in cancer therapy. As importantly, IR-HPN and IR/DOX-HPN maintained their size distribution over time, when dispersed in both water and PBS (pH 7.4), revealing an excellent colloidal stability (Fig. S4 and S5). Additionally, IR-HPN and IR/DOX-HPN presented zeta potentials of −31.3 ± 3.8 mV and −31.9 ± 0.4 mV, respectively. These values are in agreement with those reported in the literature for HA-based nanoformulations [21,27,31].

TEM analysis was also performed to characterize the morphology of IR-HPN and IR/DOX-HPN, demonstrating that both formulations have a spherical shape (Fig. S6). This morphology may be advantageous since spherical shaped-nanomaterials have been associated with augmented cellular internalization and suitable tumor homing capacity [30].

The HPN presented a similar efficiency in the encapsulation of IR780 (Fig. 1C). In fact, IR780 encapsulation in HPN could increase its water solubility up to 42.15-fold (the water solubility of IR780 is below 0.4 μg mL^{-1} [24,28]). The IR/DOX-HPN were also capable of encapsulating DOX (Fig. 1C). The LC of IR-HPN and IR/DOX-HPN is also in line with those of polymeric nanoformulations (Fig. 1D) [5,42].

3.2. NIR absorption, photothermal capability and release behaviour of IR-HPN and IR/DOX-HPN

The NIR absorption of IR-HPN and IR/DOX-HPN was then characterized to assess their ability to interact with NIR light. Free IR780 (dissolved in methanol) had a high absorption in the NIR region, revealing a maximum absorption peak at 780 nm (Fig. 1E). The encapsulation of IR780 in HPN produced a red-shift in its absorption (Fig. 1E). Due to this phenomenon, IR-HPN and IR/DOX-HPN possessed a 2.2-fold higher absorption at 808 nm than free IR780, indicating that these nanoparticles interact with 808 nm radiation, which will be used in photothermal studies. Considering that the NIR absorption spectra of disrupted IR-HPN and IR/DOX-HPN dissolved in methanol and free IR780 were similar (Fig. S7), the red-shift observed is likely to be a result from alterations in solvents' polarity or from hydrophobic-hydrophobic interactions occurring in nanoparticles' core. This red-shift of IR780 absorption when encapsulated in nanostructures was also

reported by other research groups [24,39,46,49].

Afterward, the capacity of IR-HPN and IR/DOX-HPN to convert NIR radiation into heat was investigated (Fig. S8). For such, HPN at different concentrations of IR780 were irradiated with 808 nm light during 5 min and the temperature changes were recorded (Fig. S8). For both formulations, the maximum temperature increase was achieved after 1 min of irradiation (Fig. S8). This photothermal behaviour has been associated with the photodegradation of IR780 by NIR light [38,39,48,51]. Moreover, the temperature variations induced by both formulations were similar, suggesting that the differences on HPN physicochemical properties do not affect their photothermal capability.

At the concentration of 10 $\mu g\,mL^{-1}$ (of IR780 equivalents), IR-HPN and IR/DOX-HPN induced a temperature increase of 10 °C (Fig. S8). Such temperature variation can induce cellular damages, leading to cancer cells death [9]. On the other hand, HPN produced a photoinduced heat of 4–5 °C at lower concentrations (2 and 3.5 $\mu g\,mL^{-1}$ of IR780 equivalents), which can still sensitize cancer cells to other therapeutics [15]. As importantly, the NIR radiation did not induce a significant temperature increase to water (control), which is in agreement with the weak interaction of 808 nm light with water.

In comparison to previous studies, IR-HPN and IR/DOX-HPN were able to produce a photoinduced heat (808 nm, 1.7 $W\,cm^{-2}$) of 10 °C at 10 $\mu g\,mL^{-1}$ (of IR780 equivalents), while poly(phosphorylcholine)-based micelles encapsulating IR780 induced a similar temperature increase but required a 4-times higher concentration (40 $\mu g\,mL^{-1}$ of IR780 equivalents; 808 nm, 1 $W\,cm^{-2}$) [20]. In another report, α-Lipoic acid stabilized IR780 loaded nanoformulations [29] also required a 2-times higher concentration (20 $\mu g\,mL^{-1}$ of IR780 equivalents) and a greater power density (2.5 $W\,cm^{-2}$) to induce a maximum temperature variation similar to that produced by IR780 loaded HPN (at 10 $\mu g\,mL^{-1}$ of IR780 equivalents). Together, these results confirm the photothermal capability of IR-HPN and IR/DOX-HPN.

Subsequently, the influence of the NIR radiation on IR-HPN and IR/DOX-HPN compounds' release was investigated (Fig. S9A and B). Without the presence of NIR light, IR780 was released in a sustained manner from both HPN formulations (Fig. S9A). In fact, the cumulative release of IR780 from IR-HPN and IR/DOX-HPN after 24 h was only about 7 and 21%, respectively (Fig. S9A). In other reports, the IR780 cumulative leakage from PEGylated solid lipid nanoparticles and from Pluronic F-127 micelles after 24 h was approximately 31 and 65%, respectively [26,52]. Interestingly, the NIR light did not enhance the IR780 released from HPN (Fig. S9A). Such result could be explained by the degradation of IR780 upon interaction with NIR light. To confirm this hypothesis, the absorption spectra of IR-HPN and IR/DOX-HPN before and after interaction with NIR light were acquired, which confirmed the photo-degradation of the IR780 encapsulated on HPN (Fig. S9C and D). The NIR light mediated degradation of IR780 has also been reported by other research groups [38,51]. In turn, the release of DOX from IR/DOX-HPN was responsive to the NIR radiation (Fig. S9B). In fact, the NIR light could enhance the DOX released from IR/DOX-HPN by about 3.6-fold (Fig. S9B). This result suggests that the photoinduced heat generated by IR/DOX-HPN (Fig. S8B) can destabilize the nanoparticles' structure, enabling a faster DOX release (Fig. S9B). Furthermore, these results also highlight the suitable IR780 and DOX delivery capabilities of HPN.

3.3. Cytocompatibility of IR-HPN

The encapsulation of IR780 in nanostructures can address the acute-toxicity associated with the administration of free IR780 [1]. In a previous work, we reported that the IC_{50} of IR780 towards MCF-7 cancer cells is about 10.4 $\mu g\,mL^{-1}$ [39]. Herein, we investigated the toxicity of IR-HPN towards MCF-7 cells and NHDF, as models of breast cancer and healthy cells, respectively (Fig. 2). IR-HPN did not induce meaningful variations in MCF-7 and NHDF cells' viability up to 175 $\mu g\,mL^{-1}$ of nanostructures (corresponds to an IR780 concentration of 6.88 $\mu g\,mL^{-1}$) (Fig. 2A and B). Therefore, IR780 encapsulation in HPN results in an improved cytocompatibility, a factor that is crucial for the application of these nanoformulations in cancer therapy. Moreover, the cytocompatibility of IR-HPN towards both cell lines also suggests that these nanoformulations may perform an on-demand therapy upon NIR laser irradiation.

3.4. Cellular uptake of IR-HPN and IR/DOX-HPN

After confirming the cytocompatibility of IR-HPN, the propensity of the HPN nanoformulations towards cancer cells was also assessed. For such, the intrinsic fluorescence of IR780 was explored to investigate the internalization of IR-HPN and IR/DOX-HPN by MCF-7 cells (CD44 receptor overexpressing cells [7,40,42]) and NHDF (which do not overexpress the CD44 receptor [36,50]) through CLSM. The uptake of IR/DOX-HPN by both cell lines was also visualized by using the intrinsic fluorescence of DOX.

In this context, CLSM images revealed that MCF-7 cells and NHDF incubated with free DOX displayed an unappreciable DOX fluorescence, indicating the low uptake of the free drug by these cells (Fig. S10A). In turn, IR780 fluorescence signals were observed on MCF-7 cells and NHDF incubated with free IR780 (Fig. S10B). The slightly higher IR780 fluorescence intensity observed on MCF-7 cells incubated with free IR780 may be related to the ability of this dye to target the organic anion transporter peptides (OATPs), which are overexpressed by cancer cells [1,54]. Nevertheless, the application of free IR780 in cancer on-demand phototherapy is hindered by its low solubility and high toxicity [1,39].

On the other hand, MCF-7 cells incubated with IR-HPN and IR/DOX-HPN showed a high IR780 fluorescence intensity (Fig. 3A and B). High DOX fluorescence was also observed in MCF-7 cells incubated with IR/DOX-HPN (Fig. 3B). In stark contrast, NHDF treated with the HPN formulations emitted almost no fluorescence from IR780 and DOX (Fig. 3A and B). These results indicate that HPN are more internalized by MCF-7 cells than by NHDF. Considering the composition of HPN, this effect may be mediated by the binding of the HA present on nanoparticles' corona to the CD44 receptors overexpressed on MCF-7 cells [7,40,42]. Cho et al. produced HA-based nanomedicines that also displayed a higher internalization by MCF-7 cells [7]. Therefore, the higher uptake of HPN by MCF-7 cells suggests that this formulation may be used for *in vitro* NIR imaging of this cell line and that it could be able to perform an on-demand phototherapy.

3.5. Phototherapeutic effect mediated by IR-HPN and IR/DOX-HPN in 2D cancer models

After confirming the higher uptake of IR-HPN and IR/DOX-HPN by MCF-7 cells, their phototherapeutic capability was evaluated (Fig. 4A). At the highest concentration tested (3.5 $\mu g\,mL^{-1}$ of IR780 equivalents), the combined application of NIR light and IR-HPN induced a reduction on cancer cells' viability to about 59% (Fig. 4B). Taking into account that the non-irradiated IR-HPN and the NIR radiation did not induce meaningful alterations on MCF-7 cells' viability (Fig. 4B), these results confirm that IR-HPN can induce an on-demand phototherapeutic effect.

Furthermore, IR/DOX-HPN produced a reduction of MCF-7 cells' viability to about 66% (3.5 $\mu g\,mL^{-1}$ of IR780; 1.93 $\mu g\,mL^{-1}$ of DOX). Moreover, when IR/DOX-HPN were irradiated with NIR light, a viability reduction to about 20% was attained (Fig. 4B). This outcome is likely to result from a synergic effect between DOX and IR780 (that is responsible for a temperature increase and/or reactive oxygen species production) and from the NIR light enhanced DOX release, and thus confirm the potential of the chemo-phototherapy mediated by IR/DOX-HPN.

The Calcein-AM (labels live cells) and PI (labels dead cells) stainings were also performed to visualize the phototherapeutic capabilities of HPN (Fig. 4C–D). As expected, the sole application of NIR light or non-

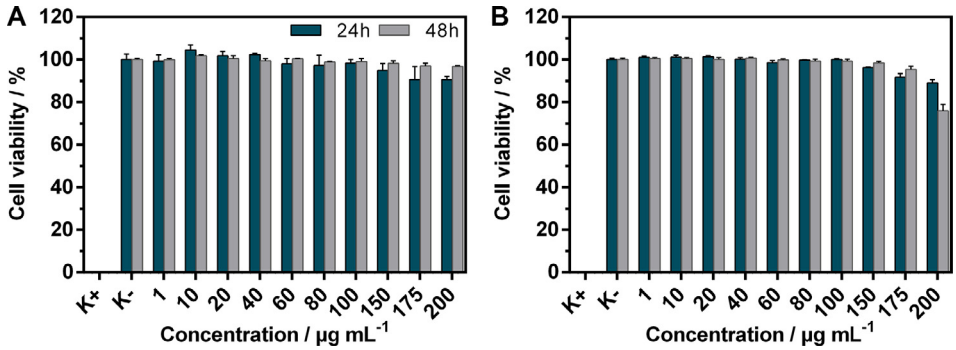

Fig. 2. Evaluation of the cytocompatibility of IR-HPN. MCF-7 cells (A) and NHDF (B) were incubated with different concentrations of IR-HPN during 24 and 48 h. K- and K+ represent the negative and the positive controls, respectively. Each bar represents the mean ± S.D. (n = 5).

irradiated IR-HPN did not induce considerable cytotoxicity towards MCF-7 cells (Fig. 4C–D). On the other hand, the administration of IR/DOX-HPN and the conjugation of IR-HPN or IR/DOX-HPN with NIR light led to cells' death (Fig. 4C–D). In this regard, the highest number of dead cells was induced by the combination of IR/DOX-HPN with NIR (Fig. 4C–D), further corroborating the superior efficacy of the chemo-phototherapy mediated by this nanoformulation.

Han et al. previously reported that the therapeutic effect induced by poly(phosphorylcholine)-based micelles encapsulating IR780 was improved by 1.32-fold upon exposure to NIR light (808 nm, 0.6 W cm^{-2}, 10 min) [20], while the irradiation of IR-HPN improved their therapeutic capacity by 1.54-fold (808 nm, 1.7 W cm^{-2}, 5 min). In another work, the combined application of NIR light and α-Lipoic acid stabilized-based nanoformulations loaded with Docetaxel and IR780 improved the therapeutic outcome by up to 3.26-fold [29]. In this work, a 3.35-times higher therapeutic efficacy was attained when combining NIR light and IR/DOX-HPN, which is a similar effect to that of the previous report [29]. However, in the case of IR/DOX-HPN, a lower

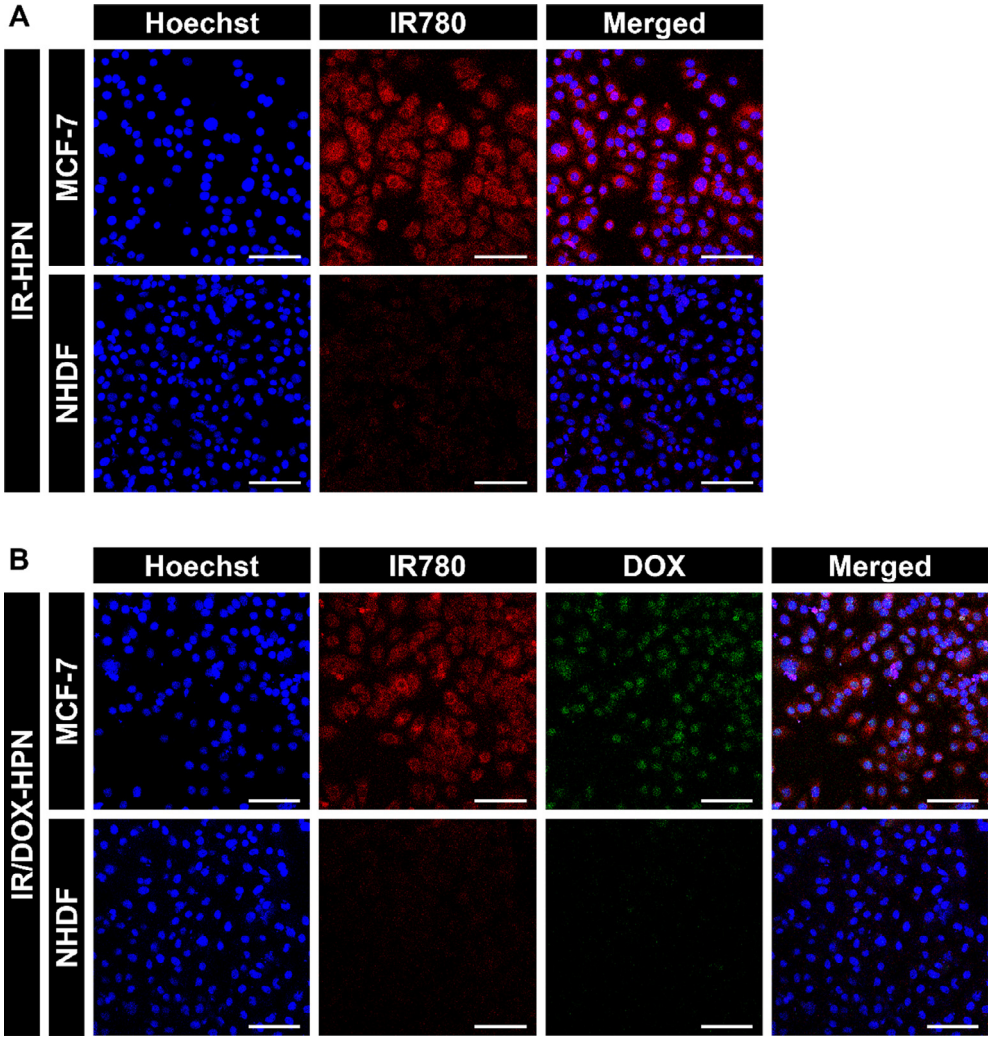

Fig. 3. Determination of HPN internalization. Cellular uptake of IR-HPN (A) and IR/DOX-HPN (B) by MCF-7 cells and NHDF. Blue channel: Hoechst 33342® stained nucleus; Green channel: DOX; Red channel: IR780. Scale bars correspond to 100 μm.

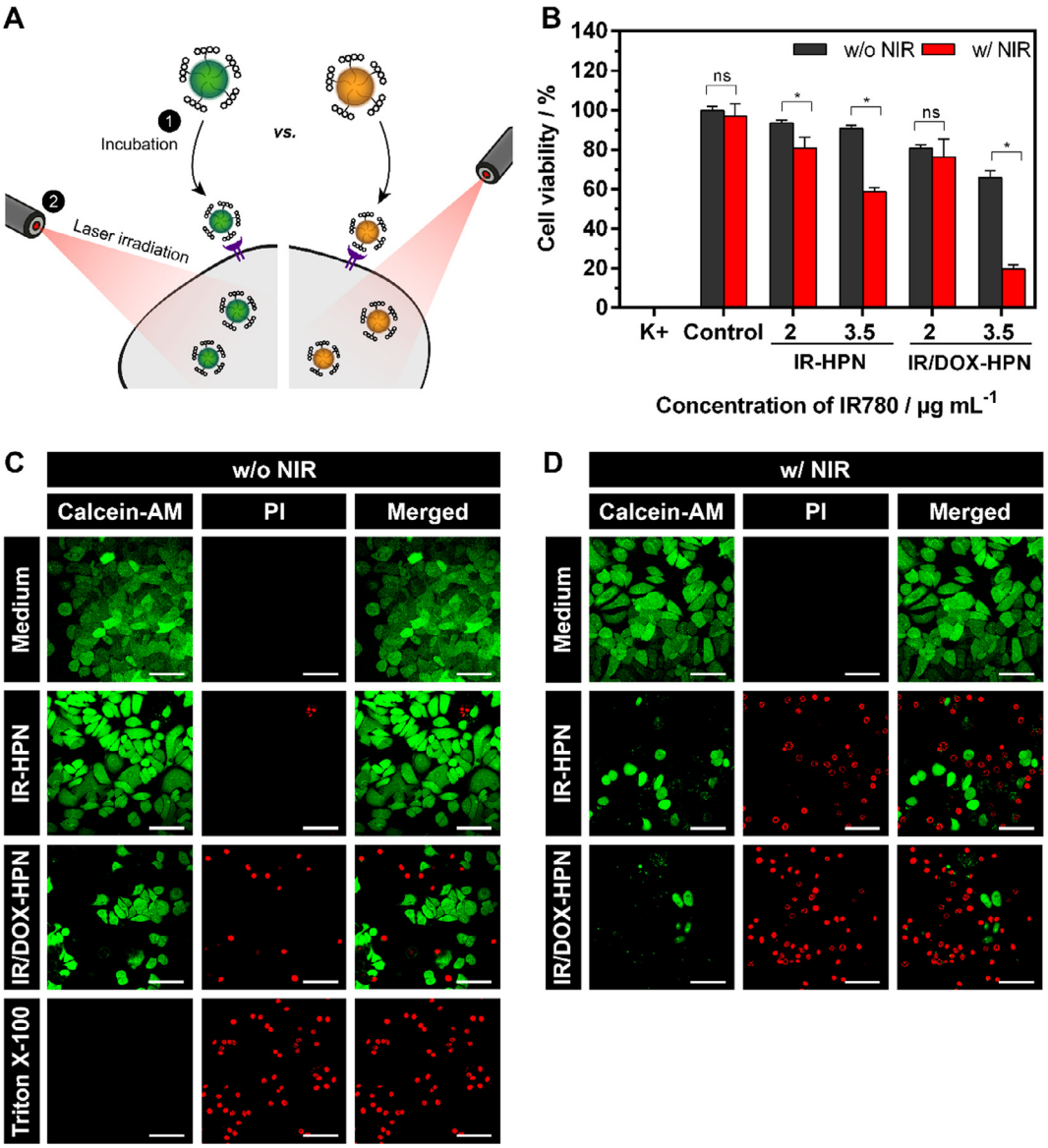

Fig. 4. Determination of the therapeutic capacity of IR-HPN and IR/DOX-HPN in 2D MCF-7 cells. Schematic representation of the procedure used to evaluate the phototherapeutic effect of IR-HPN or IR/DOX-HPN towards MCF-7 cells (A). Therapeutic effect mediated by HPN towards MCF-7 cells without (w/o NIR) and with NIR (w/ NIR) laser irradiation (808 nm, 1.7 W cm^{-2}, 5 min) (B). K+ represents the positive control. Control w/o NIR represents the negative control, while control w/ NIR represents cells solely treated with NIR light. Data represents mean ± S.D., n = 5, (*$p < 0.0001$), ns = non-significant. CLSM images of MCF-7 cells stained with Calcein-AM/PI after treatment with HPN w/o (C) or w/ NIR (D) laser irradiation (808 nm, 1.7 W cm^{-2}, 5 min). Medium w/o NIR and Triton X-100 w/o NIR represent the live and dead cells controls, respectively. Medium w/ NIR represents cells solely treated with NIR light. Green channel: Calcein-AM; Red channel: PI. Scale bars correspond to 100 μm.

drug dose (1.93 *vs.* 12.5 μg mL^{-1}) and a weaker intensity (1.7 *vs.* 2.5 W cm^{-2}; 5 min) were required to achieve such effect [29].

3.6. Penetration and phototherapeutic effect mediated by IR-HPN and IR/DOX-HPN in 3D cancer models

After confirming the phototherapeutic capability of HPN in 2D cultures of MCF-7 cells, their efficacy was assessed in 3D spheroids. Spheroids can mimic many features of the *in vivo* solid tumors, namely their 3D structure, layered cellular organization, resistance to therapeutics, among others [11,34]. The cell-cell and cell-extracellular matrix interactions of *in vivo* tumors are also mimicked by spheroids, constituting a physical barrier to the penetration of therapeutics [11,34]. Due to these reasons, spheroids are a prime *in vitro* model for evaluating the anticancer capacity of nanomaterials [18,22,37].

Initially, the intrinsic fluorescence of IR780 was explored to analyse the distribution of IR-HPN and IR/DOX-HPN within the 3D MCF-7 spheroids by CLSM (Fig. S11). Fluorescence signals were observed in the spheroids at different penetration depths, indicating the capacity of HPN to penetrate into these 3D *in vitro* microtissues (Fig. S11). Furthermore, the plots of the fluorescence intensity across the spheroids' diameter revealed that HPN remained mostly in the spheroids' periphery and that some nanostructures were able to reach the spheroids' core (Fig. S11). The higher accumulation of the nanostructures in the spheroids' outer layers was also reported by other research groups [4,17,22].

Then, the phototherapeutic capability of HPN in 3D MCF-7 spheroids was assessed (Fig. 5A). In agreement with the results obtained in the 2D cancer models, the non-irradiated IR-HPN and the sole application of NIR light did not produce any cytotoxic effect on spheroids (Fig. 5B). Moreover, IR/DOX-HPN were capable of reducing spheroids cells' viability to 54% (Fig. 5B). In turn, the combination of IR/DOX-

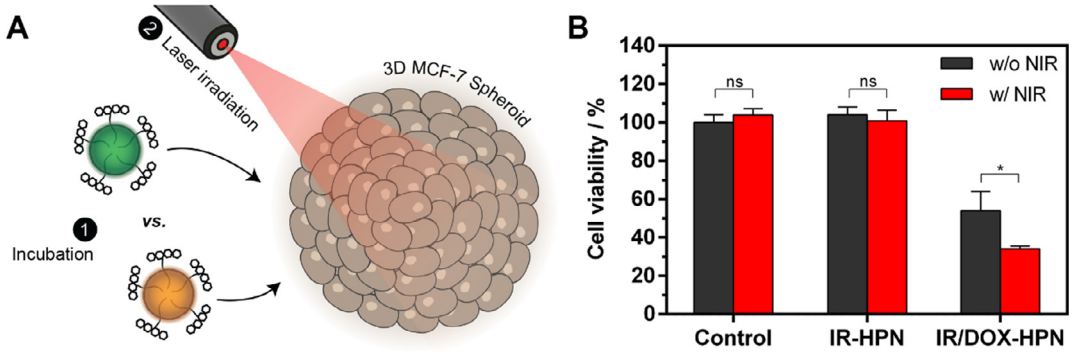

Fig. 5. Determination of the therapeutic capacity of IR-HPN and IR/DOX-HPN in 3D MCF-7 spheroids. Schematic representation of the procedure used to evaluate the phototherapeutic effect of IR-HPN or IR/DOX-HPN towards 3D MCF-7 spheroids (A). Therapeutic effect mediated by HPN towards MCF-7 spheroids without (w/o NIR) and with NIR (w/ NIR) laser irradiation (808 nm, 1.7 W cm^{-2}, 5 min) (B). Control w/o NIR represents the negative control, while control w/ NIR represents spheroids solely treated with NIR light. Data represents mean ± S.D., n = 30, (*$p < 0.0001$), ns = non-significant.

HPN and NIR light further decreased spheroids cells' viability to about 34%, resulting in the most prominent therapeutic effect (Fig. 5B). Surprisingly, the combined action of IR-HPN and NIR light did not induce cytotoxicity towards the spheroids (Fig. 5B). This effect diverges from that attained in the 2D *in vitro* models (Fig. 4B), suggesting that spheroids are less affected by the action of the photoactivated IR-HPN. Such result can be explained by the higher resistance of spheroids to temperature- and reactive oxygen species-mediated cell death [25,47]. Moreover, the effect of therapeutics on spheroids is also generally inferior to that occurring in the 2D cancer cells [23,35,43]. In this way, these results also highlight the importance of using 3D spheroids for the screening of anticancer phototherapies. Overall, IR/DOX-HPN revealed promising properties for being applied in cancer chemo-phototherapy.

4. Conclusion

In this work, HA-*g*-PMAO was explored for the first time in the preparation of polymeric nanoparticles encapsulating IR780 and DOX aimed for breast cancer chemo-phototherapy. The results revealed that IR-HPN and IR/DOX-HPN with suitable physicochemical properties could be prepared by using the nanoprecipitation method. The encapsulation of IR780 in HPN improved its absorption at 808 nm by about 2.2-fold, thereby enhancing its photothermal potential. Furthermore, loading IR780 in HPN also improved its cytocompatibility. The 2D *in vitro* cell uptake studies revealed that the nanostructures displayed a higher internalization by breast cancer cells than by normal cells. In addition, the assays performed in 3D *in vitro* models of breast cancer revealed that HPN can penetrate into spheroids. Furthermore, the 3D *in vitro* studies also demonstrated that the combined application of IR-HPN and NIR light was unable to induce cytotoxicity on spheroids. In contrast, IR/DOX-HPN produced a decrease on spheroids cells' viability to 54%. Moreover, the combined action of IR/DOX-HPN and NIR light induced an even stronger therapeutic effect by reducing spheroids cells' viability to 34%. Overall, IR/DOX-HPN are promising nanoformulations for cancer chemo-phototherapy. In the future, the evaluation of the *in vivo* behaviour of these nanoformulations will fully disclose their diagnosis and therapeutic potentials.

Declaration of interest

Declarations of interest: none.

Acknowledgments

Ricardo O. Louro is acknowledged for helpful comments and suggestions. This work was supported by FEDER funds through the POCI – COMPETE 2020 – Operational Programme Competitiveness and Internationalization in Axis I – Strengthening research, technological development and innovation (Project POCI-01-0145-FEDER-007491) and National Funds by FCT – Foundation for Science and Technology (Project UID/Multi/00709/2013). The funding from CENTRO-01-0145-FEDER-028989 is also acknowledged. Duarte de Melo-Diogo and Elisabete C. Costa acknowledge individual PhD fellowships from FCT (SFRH/BD/103506/2014 and SFRH/BD/103507/2014). Duarte de Melo-Diogo also acknowledges CENTRO-01-0145-FEDER-028989 for the funding given on the form of a research contract.

Appendix A. Supplementary material

Supplementary data to this article can be found online at https://doi.org/10.1016/j.ejpb.2019.02.016.

References

[1] C.G. Alves, R. Lima-Sousa, D. de Melo-Diogo, R.O. Louro, I.J. Correia, IR780 based nanomaterials for cancer imaging and photothermal, photodynamic and combinatorial therapies, Int. J. Pharm. 542 (2018) 164–175.
[2] E. Blanco, H. Shen, M. Ferrari, Principles of nanoparticle design for overcoming biological barriers to drug delivery, Nat. Biotechnol. 33 (2015) 941–951.
[3] Y. Chen, Z. Li, H. Wang, Y. Wang, H. Han, Q. Jin, J. Ji, IR-780 loaded phospholipid mimicking homopolymeric micelles for near-IR imaging and photothermal therapy of pancreatic cancer, ACS Appl. Mater. Interf. 8 (2016) 6852–6858.
[4] Y. Chen, W. Zhang, Y. Huang, F. Gao, X. Fang, Dual-functional c(RGDyK)-decorated Pluronic micelles designed for antiangiogenesis and the treatment of drug-resistant tumor, Int. J. Nanomed. 10 (2015) 4863–4881.
[5] S. Cheon Lee, C. Kim, I. Chan Kwon, H. Chung, S. Young Jeong, Polymeric micelles of poly(2-ethyl-2-oxazoline)-block-poly(epsilon-caprolactone) copolymer as a carrier for paclitaxel, J. Control. Release 89 (2003) 437–446.
[6] M. Chidambaram, R. Manavalan, K. Kathiresan, Nanotherapeutics to overcome conventional cancer chemotherapy limitations, J. Pharm. Pharmaceut. Sci. 14 (2011) 67–77.
[7] H.J. Cho, H.Y. Yoon, H. Koo, S.H. Ko, J.S. Shim, J.H. Lee, K. Kim, I.C. Kwon, D.D. Kim, Self-assembled nanoparticles based on hyaluronic acid-ceramide (HA-CE) and Pluronic(R) for tumor-targeted delivery of docetaxel, Biomaterials 32 (2011) 7181–7190.
[8] K.Y. Choi, H. Chung, K.H. Min, H.Y. Yoon, K. Kim, J.H. Park, I.C. Kwon, S.Y. Jeong, Self-assembled hyaluronic acid nanoparticles for active tumor targeting, Biomaterials 31 (2010) 106–114.
[9] K.F. Chu, D.E. Dupuy, Thermal ablation of tumours: biological mechanisms and advances in therapy, Nat. Rev. Cancer 14 (2014) 199–208.
[10] E.C. Costa, A.F. Moreira, D. de Melo-Diogo, I.J. Correia, ClearT immersion optical clearing method for intact 3D spheroids imaging through confocal laser scanning microscopy, Opt. Laser Technol. 106 (2018) 94–99.
[11] E.C. Costa, A.F. Moreira, D. de Melo-Diogo, V.M. Gaspar, M.P. Carvalho, I.J. Correia, 3D tumor spheroids: an overview on the tools and techniques used for their analysis, Biotechnol. Adv. 34 (2016) 1427–1441.
[12] E.C. Costa, A.F. Moreira, D.D. Melo-Diogo, I.J. Correia 2018b. Polyethylene glycol molecular weight influences the Clear < sup > T2 < /sup > optical clearing method for spheroids imaging by confocal laser scanning microscopy. SPIE, p. 11.
[13] D. de Melo-Diogo, E.C. Costa, C.G. Alves, R. Lima-Sousa, P. Ferreira, R.O. Louro, I.J. Correia, POxylated graphene oxide nanomaterials for combination chemo-phototherapy of breast cancer cells, Eur. J. Pharm. Biopharm. : Off. J. Arbeitsgemeinschaft fur Pharmazeutische Verfahrenstechnik e.V 131 (2018) 162–169.

[14] D. de Melo-Diogo, C. Pais-Silva, E.C. Costa, R.O. Louro, I.J. Correia, D-α-tocopheryl polyethylene glycol 1000 succinate functionalized nanographene oxide for cancer therapy, Nanomedicine (London, England) 12 (2017) 443–456.
[15] D. de Melo-Diogo, C. Pais-Silva, D.R. Dias, A.F. Moreira, I.J. Correia, Strategies to improve cancer photothermal therapy mediated by nanomaterials, Adv. Healthc. Mater. 6 (2017).
[16] J. Ferlay, I. Soerjomataram, R. Dikshit, S. Eser, C. Mathers, M. Rebelo, D.M. Parkin, D. Forman, F. Bray, Cancer incidence and mortality worldwide: sources, methods and major patterns in GLOBOCAN 2012, Int. J. Cancer 136 (2015) E359–E386.
[17] Y. Gao, M. Li, B. Chen, Z. Shen, P. Guo, M.G. Wientjes, J.L.S. Au, Predictive models of diffusive nanoparticle transport in 3-dimensional tumor cell spheroids, AAPS J. 15 (2013) 816–831.
[18] V.M. Gaspar, P. Baril, E.C. Costa, D. de Melo-Diogo, F. Foucher, J.A. Queiroz, F. Sousa, C. Pichon, I.J. Correia, Bioreducible poly(2-ethyl-2-oxazoline)–PLA–PEI-SS triblock copolymer micelles for co-delivery of DNA minicircles and Doxorubicin, J. Control. Release 213 (2015) 175–191.
[19] V.M. Gaspar, C. Gonçalves, D. de Melo-Diogo, E.C. Costa, J.A. Queiroz, C. Pichon, F. Sousa, I.J. Correia, Poly(2-ethyl-2-oxazoline)–PLA-g–PEI amphiphilic triblock micelles for co-delivery of minicircle DNA and chemotherapeutics, J. Control. Release 189 (2014) 90–104.
[20] H. Han, S. Zhang, Y. Wang, T. Chen, Q. Jin, Y. Chen, Z. Li, J. Ji, Biomimetic drug nanocarriers prepared by miniemulsion polymerization for near-infrared imaging and photothermal therapy, Polymer 82 (2016) 255–261.
[21] J. Huang, H. Zhang, Y. Yu, Y. Chen, D. Wang, G. Zhang, G. Zhou, J. Liu, Z. Sun, D. Sun, Y. Lu, Y. Zhong, Biodegradable self-assembled nanoparticles of poly (D, L-lactide-co-glycolide)/hyaluronic acid block copolymers for target delivery of docetaxel to breast cancer, Biomaterials 35 (2014) 550–566.
[22] K. Huang, H. Ma, J. Liu, S. Huo, A. Kumar, T. Wei, X. Zhang, S. Jin, Y. Gan, P.C. Wang, S. He, X. Zhang, X.J. Liang, Size-dependent localization and penetration of ultrasmall gold nanoparticles in cancer cells, multicellular spheroids, and tumors in vivo, ACS Nano 6 (2012) 4483–4493.
[23] Y. Imamura, T. Mukohara, Y. Shimono, Y. Funakoshi, N. Chayahara, M. Toyoda, N. Kiyota, S. Takao, S. Kono, T. Nakatsura, H. Minami, Comparison of 2D- and 3D-culture models as drug-testing platforms in breast cancer, Oncol. Rep. 33 (2015) 1837–1843.
[24] C. Jiang, H. Cheng, A. Yuan, X. Tang, J. Wu, Y. Hu, Hydrophobic IR780 encapsulated in biodegradable human serum albumin nanoparticles for photothermal and photodynamic therapy, Acta Biomater. 14 (2015) 61–69.
[25] S. Khoei, B. Goliaei, A. Neshasteh-Riz, Differential thermo-resistance of multicellular tumor spheroids, Iran. J. Sci. Technol. (Sciences) 28 (2004) 107–116.
[26] Y. Kuang, K. Zhang, Y. Cao, X. Chen, K. Wang, M. Liu, R. Pei, Hydrophobic IR-780 dye encapsulated in cRGD-conjugated solid lipid nanoparticles for NIR imaging-guided photothermal therapy, ACS Appl. Mater. Interf. 9 (2017) 12217–12226.
[27] J. Li, M. Huo, J. Wang, J. Zhou, J.M. Mohammad, Y. Zhang, Q. Zhu, A.Y. Waddad, Q. Zhang, Redox-sensitive micelles self-assembled from amphiphilic hyaluronic acid-deoxycholic acid conjugates for targeted intracellular delivery of paclitaxel, Biomaterials 33 (2012) 2310–2320.
[28] S. Li, S. Zhou, Y. Li, X. Li, J. Zhu, L. Fan, S. Yang, Exceptionally high payload of the IR780 iodide on folic acid-functionalized graphene quantum dots for targeted photothermal therapy, ACS Appl. Mater. Interf. 9 (2017) 22332–22341.
[29] W. Li, J. Peng, Q. Yang, L. Chen, L. Zhang, X. Chen, Z. Qian, α-Lipoic acid stabilized DTX/IR780 micelles for photoacoustic/fluorescence imaging guided photothermal therapy/chemotherapy of breast cancer, Biomater. Sci. 6 (2018) 1201–1216.
[30] Y. Li, M. Kroger, W.K. Liu, Shape effect in cellular uptake of PEGylated nanoparticles: comparison between sphere, rod, cube and disk, Nanoscale 7 (2015) 16631–16646.
[31] R. Lima-Sousa, D. de Melo-Diogo, C.G. Alves, E.C. Costa, P. Ferreira, R.O. Louro, I.J. Correia, Hyaluronic acid functionalized green reduced graphene oxide for targeted cancer photothermal therapy, Carbohydr. Polym. 200 (2018) 93–99.
[32] R. Lin, L. Shi Ng, C.-H. Wang, In vitro study of anticancer drug doxorubicin in PLGA-based microparticles, Biomaterials 26 (2005) 4476–4485.
[33] S.Y. Lin, R.Y. Huang, W.C. Liao, C.C. Chuang, C.W. Chang, Multifunctional PEGylated albumin/IR780/iron oxide nanocomplexes for cancer photothermal therapy and MR imaging, Nanotheranostics 2 (2018) 106–116.
[34] G. Mehta, A.Y. Hsiao, M. Ingram, G.D. Luker, S. Takayama, Opportunities and challenges for use of tumor spheroids as models to test drug delivery and efficacy, J. Control. Release 164 (2012) 192–204.
[35] A.S. Mikhail, S. Eetezadi, C. Allen, Multicellular tumor spheroids for evaluation of cytotoxicity and tumor growth inhibitory effects of nanomedicines in vitro: a comparison of docetaxel-loaded block copolymer micelles and taxotere®, PLoS ONE 8 (2013) e62630.
[36] Y. Miyatake, A.L.A. Oliveira, M.A. Jarboui, S. Ota, U. Tomaru, T. Teshima, W.W. Hall, M. Kasahara, Protective roles of epithelial cells in the survival of adult T-cell leukemia/lymphoma cells, Am. J. Pathology 182 (2013) 1832–1842.
[37] A.F. Moreira, D.R. Dias, E.C. Costa, I.J. Correia, Thermo- and pH-responsive nano-in-micro particles for combinatorial drug delivery to cancer cells, Eur. J. Pharm. Sci. 104 (2017) 42–51.
[38] T. Nagy-Simon, M. Potara, A.M. Craciun, E. Licarete, S. Astilean, IR780-dye loaded gold nanoparticles as new near infrared activatable nanotheranostic agents for simultaneous photodynamic and photothermal therapy and intracellular tracking by surface enhanced resonant Raman scattering imaging, J. Colloid Interf. Sci. 517 (2018) 239–250.
[39] C. Pais-Silva, D. de Melo-Diogo, I.J. Correia, IR780-loaded TPGS-TOS micelles for breast cancer photodynamic therapy, Eur. J. Pharm. Biopharm. 113 (2017) 108–117.
[40] V.M. Platt, F.C. Szoka Jr., Anticancer therapeutics: targeting macromolecules and nanocarriers to hyaluronan or CD44, a hyaluronan receptor, Mol. Pharm. 5 (2008) 474–486.
[41] J. Qi, P. Yao, F. He, C. Yu, C. Huang, Nanoparticles with dextran/chitosan shell and BSA/chitosan core—Doxorubicin loading and delivery, Int. J. Pharm. 393 (2010) 177–185.
[42] L. Qiu, Z. Li, M. Qiao, M. Long, M. Wang, X. Zhang, C. Tian, D. Chen, Self-assembled pH-responsive hyaluronic acid-g-poly((L)-histidine) copolymer micelles for targeted intracellular delivery of doxorubicin, Acta Biomater 10 (2014) 2024–2035.
[43] C. Sarisozen, S. Dhokai, E.G. Tsikudo, E. Luther, I.M. Rachman, V.P. Torchilin, Nanomedicine based curcumin and doxorubicin combination treatment of glioblastoma with scFv-targeted micelles: in vitro evaluation on 2D and 3D tumor models, Eur. J. Pharm. Biopharm. 108 (2016) 54–67.
[44] T.H. Tran, H.T. Nguyen, T.T.P. Tran, S.K. Ku, J.-H. Jeong, H.-G. Choi, C.S. Yong, J.O. Kim, Combined photothermal and photodynamic therapy by hyaluronic acid-decorated polypyrrole nanoparticles, Nanomedicine 12 (2017) 1511–1523.
[45] M. Uchino, H. Kojima, K. Wada, M. Imada, F. Onoda, H. Satofuka, T. Utsugi, Y. Murakami, Nuclear β-catenin and CD44 upregulation characterize invasive cell populations in non-aggressive MCF-7 breast cancer cells, BMC Cancer 10 (2010) 414.
[46] K. Wang, Y. Zhang, J. Wang, A. Yuan, M. Sun, J. Wu, Y. Hu, 2016. Self-assembled IR780-loaded transferrin nanoparticles as an imaging, targeting and PDT/PTT agent for cancer therapy.
[47] Y. Xu, T. Shi, A. Xu, L. Zhang, 3D spheroid culture enhances survival and therapeutic capacities of MSCs injected into ischemic kidney, J. Cell Mol. Med. 20 (2016) 1203–1213.
[48] F. Yan, W. Duan, Y. Li, H. Wu, Y. Zhou, M. Pan, H. Liu, X. Liu, H. Zheng, NIR-laser-controlled drug release from DOX/IR-780-loaded temperature-sensitive-liposomes for chemo-photothermal synergistic tumor therapy, Theranostics 6 (2016) 2337–2351.
[49] L. Yan, H. Wang, A. Zhang, C. Zhao, Y. Chen, X. Li, Bright and stable near-infrared Pluronic-silica nanoparticles as contrast agents for in vivo optical imaging, J. Mater. Chem. B 4 (2016) 5560–5566.
[50] C. Yang, Y. He, H. Zhang, Y. Liu, W. Wang, Y. Du, F. Gao, Selective killing of breast cancer cells expressing activated CD44 using CD44 ligand-coated nanoparticles in vitro and in vivo, Oncotarget 6 (2015) 15283–15296.
[51] A. Yuan, X. Qiu, X. Tang, W. Liu, J. Wu, Y. Hu, Self-assembled PEG-IR-780-C13 micelle as a targeting, safe and highly-effective photothermal agent for in vivo imaging and cancer therapy, Biomaterials 51 (2015) 184–193.
[52] Y. Zhan, X. Cao, Y. Li, J. Tian, J. Liang, X. Chen, Silica cross-linked micellar core-shell nanoparticles encapsulating IR-780 with strong bright and good biocompatibility for optical imaging in vivo, J. Biomed. Nanotechnol. 13 (2017) 144–154.
[53] C. Zhang, S. Wang, J. Xiao, X. Tan, Y. Zhu, Y. Su, T. Cheng, C. Shi, Sentinel lymph node mapping by a near-infrared fluorescent heptamethine dye, Biomaterials 31 (2010) 1911–1917.
[54] E. Zhang, S. Luo, X. Tan, C. Shi, Mechanistic study of IR-780 dye as a potential tumor targeting and drug delivery agent, Biomaterials 35 (2014) 771–778.